THE JOURNAL OF PHYSICAL CHEMISTRY C

Article

Cite This: J. Phys. Chem. C 2018, 122, 15297−15303

pubs.acs.org/JPCC

Indirect-to-Direct Band Gap Transition of Si Nanosheets: Effect of Biaxial Strain

Byung-Hyun Kim,[†,‡,§,⊥] Mina Park,[‡,⊥] Gyubong Kim,[‡] Kersti Hermansson,[§] Peter Broqvist,[§] Heon-Jin Choi,[∥] and Kwang-Ryeol Lee*[,‡]

[†]R&D Platform Center, Korea Institute of Energy Research, 34129 Daejeon, Republic of Korea

[‡]Computational Science Research Center, Korea Institute of Science and Technology, 02792 Seoul, Republic of Korea

[§]Department of Chemistry-Ångström Laboratory, Uppsala University, Box 538, S-751 21 Uppsala, Sweden

[∥]Department of Materials Science and Engineering, Yonsei University, 262 Seongsanno, Seodaemun-Gu, 120-749 Seoul, Republic of Korea

Supporting Information

ABSTRACT: The effect of biaxial strain on the band structure of two-dimensional silicon nanosheets (Si NSs) with (111), (110), and (001) exposed surfaces was investigated by means of density functional theory calculations. For all the considered Si NSs, an indirect-to-direct band gap transition occurs as the lateral dimensions of Si NSs increase; that is, increasing lateral biaxial strain from compressive to tensile always enhances the direct band gap characteristics. Further analysis revealed the mechanism of the transition which is caused by preferential shifts of the conduction band edge at a specific *k*-point because of their bond characteristics. Our results explain a photoluminescence result of the (111) Si NSs [U. Kim et al., *ACS Nano* **2011**, *5*, 2176−2181] in terms of the plausible tensile strain imposed in the unoxidized inner layer by surface oxidation.

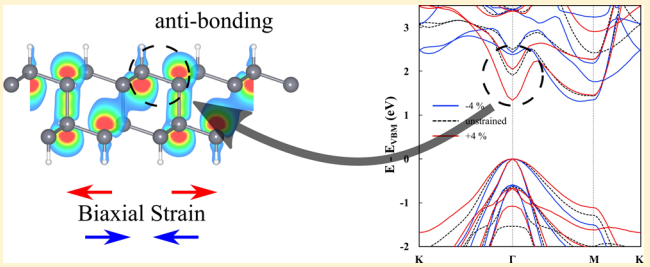

INTRODUCTION

Two-dimensional nanomaterials such as graphene,[1,2] boron nitride,[3,4] and MoS_2[5,6] have attracted great attention owing to their exceptional and tuneable properties, which are distinguishable from those of their bulk phases. Recently, layered Si nanostructures, referred to as Si nanosheets (Si NSs), have been synthesized by allowing polysilane to react with a Grignard reagent,[7−11] chemical reduction processes,[12] or chemical vapor deposition processes.[13−15] Compared to other materials, Si-based nanostructures have great advantages when it comes to commercialization, as Si is compatible with the conventional device manufacturing processes in the microelectronics industry.[16−18]

In experiments, only Si NSs exposing the (111) surface (hereafter referred to as (111) Si NSs) have been synthesized successfully so far, while those exposing surfaces of other orientations [e.g. (110) and (001)] could not be stabilized. Kim et al. performed photoluminescence measurements on free-standing (111) Si NSs and showed thickness-dependent light emissions in the visible wavelength regime, originating from quantum confinement effects.[13,14] This observation indicates that thin (111) Si NSs have a direct band gap, whereas bulk Si normally has an indirect band gap. These measurements support the prior findings of Sugiyama et al., who reported on a light-induced photocurrent from organosilicon NSs, which is indicative of a direct band gap transition.[10] However, in these reports, they leave the question of the physical origin behind this nanoeffect of Si unanswered.

The observed behavior of light emission or photocurrent is rather puzzling if one considers the band dispersion of Si NSs. Using theoretical calculations, Morishita et al. showed that bilayered (111) Si NSs have an indirect band gap, regardless of doping by hydrogen or phosphorus.[19] Wang et al. reported band gaps of hydrogenated Si NSs with varying the number of atomic layers[20] and found that the (111) Si NSs have an indirect band gap (see Figure 3 of ref 20) for all the investigated thicknesses (up to 8 Si layers). Both these studies are in disagreement with the light emission or photocurrent experiments discussed above. Interestingly, when it comes to other NS orientations, Zhang et al. studied the band dispersion of (110) and (001) Si NSs and found that these NSs have direct band gaps.[21] Furthermore, for the (110) and (001) orientations, Zhang et al. additionally reported that there is a direct-to-indirect band gap transition occurring when the NS is strained. These NS orientations are however unstable and cannot be synthesized in experiments, but the results show that the strain can have notable effects on the band structure. So far, the strain effect on the more experimentally relevant (111) Si NSs has not been fully investigated.

Received: March 6, 2018
Revised: May 28, 2018
Published: May 31, 2018

DOI: 10.1021/acs.jpcc.8b02239
J. Phys. Chem. C 2018, 122, 15297−15303

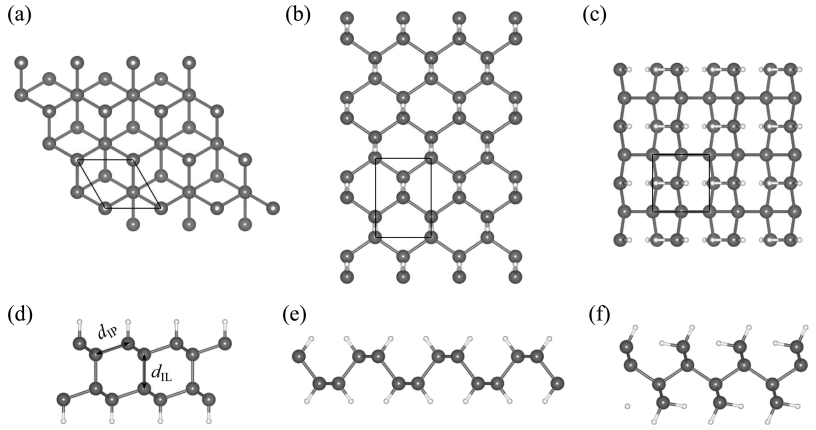

Figure 1. Model structures of bilayered Si NSs with hydrogen passivation. Top and side views of (a,d) (111)-, (b,e) (110)-, and (c,f) (001)-oriented Si NSs. Dark grey and white balls represent Si and O atoms, respectively. The black boxes indicate the supercells used in this work. d_{IP} and d_{IL} indicate the in-plane and interlayer distances, respectively.

Applying external stress, that is, strain engineering, has been widely used to control the electronic structure and thus the electronic properties of Si nanomaterials. Additionally, any external perturbation, such as surface functionalization or oxidation of Si nanomaterials can generate strain. For example, Si nanowires (Si NWs) tend to form an amorphous SiO_2 layer of 1−2 nm thickness when exposed to air. This oxidation results in compressive radial strain and tensile axial strain.[22] Molecular dynamics (MD) simulations[23,24] and continuum modeling[25] of oxidized Si NWs suggest that the oxidation induces strain in the order of a few percent in the Si layers. Previous theoretical calculations have shown that this externally induced strain can cause an indirect-to-direct band gap transition in Si NWs.[26−29] In microelectronic applications, strained ultrathin Si has been used in the channel of the metal-oxide-semiconductor field effect transistors to enhance the carrier mobility.[30,31] Thus, understanding the effect that strain has on the electronic structure of Si nanomaterials is not only of academic interest but important for practical applications of Si-based nanodevices in general.

In the present work, we focus on the effect that strain has on the band dispersion in Si NSs, by means of density functional theory (DFT) calculations. Even though only (111) Si NSs have been experimentally synthesized, we here also investigate the behavior of the (110) and (001) Si NSs to obtain a comprehensive view of strain effects in Si nanostructures. The main result of our analysis reveals a general trend of an indirect-to-direct transition upon increasing lateral biaxial stress: increasing the lateral dimensions of the NSs enhances the direct band gap characteristics for all investigated Si NSs in the present work. An unstrained (111) Si NS has an indirect band gap but yields an indirect-to-direct band gap transition when the tensile strain in the NS is larger than a critical value. For the (110) and (001) Si NSs, the critical strain was found to be negative; that is, an unstrained Si NS has a direct band gap and yields a direct-to-indirect band gap transition under compressive strain. The results provide a clue to understand experimental observations of efficient light emission from (111) Si NSs.[13,14]

COMPUTATIONAL METHODS

The electronic structure calculations were performed using the DFT as implemented in the Vienna Ab Initio Simulation Package.[32] In the calculations, we used projector augmented wave pseudopotentials,[33] explicitly treating the H 1s and the Si 3s3p electrons. The electron exchange−correlation energy was described within the generalized gradient approximation as proposed by Perdew−Burke−Ernzerhof.[34] The Kohn−Sham single-electron wave functions were expanded using a plane wave basis set, truncated with an energy cut-off of 400 eV. The Brillouin zone was sampled using the Monkhorst−Pack sampling[35] with 8 × 8 × 1 k-points. It is widely known that DFT calculations underestimate band gaps of semiconductors and insulators. However, DFT calculations are still instrumental in predicting trends of band gap changes and capable of demonstrating the physical mechanism behind such trends.

Figure 1 shows the atomic models of Si NSs with the three different exposed surface orientations investigated in this work: the (111), (110), and (001). The Si NSs were modeled with 1 to 10 layers of Si, and all surface Si dangling bonds were passivated with hydrogen atoms. The normal to the exposed surface was always aligned along the z direction of the supercell. Periodic boundary conditions were applied to the x and y directions while the NSs were separated by a large vacuum gap (in the z direction), ∼10 Å, to ensure minimal interaction between the sheets. The unstrained Si NSs were generated by a full relaxation of all atoms and the lattice parameter in x and y directions. Biaxial lattice strain was thereafter imposed by changing the dimensions of the supercell in both x and y directions simultaneously. In the following, the strain is given in percentage with respect to the fully relaxed NS lattice parameters. For all presented structures, the internal coordinates were fully relaxed until the maximal force on each atom was less than 0.01 eV/Å. Note that the range of imposed strain we used in this work, ±7%, was found to be within the elastic region as shown in Figure S1 in the Supporting Information.

Because spontaneous oxidation of Si always occurs at ambient conditions resulting in a thin native oxide layer on the Si surface, we additionally conducted reactive MD simulations of Si NS oxidation using a reactive force field (ReaxFF, ref 36) to further understand the effect that surface oxidation has on the strain evolution in Si NSs. The simulations were made using the "Large-scale Atomic/Molecular Massively Parallelized Simulator" program.[37] The MD time step was set to 1 fs to ensure smooth simulations, that is, to avoid drifts in conserved energy contributions. To describe the Si−O interactions, we used a previously developed force-field[38]

DOI: 10.1021/acs.jpcc.8b02239
J. Phys. Chem. C 2018, 122, 15297−15303

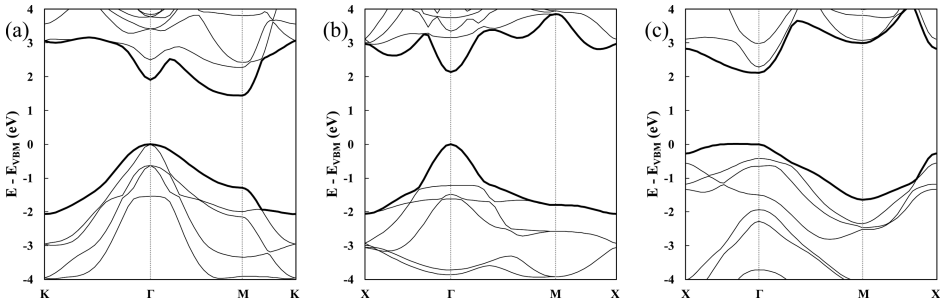

Figure 2. Band structures of unstrained bilayered Si NSs of (a) (111), (b) (110), and (c) (001) orientations.

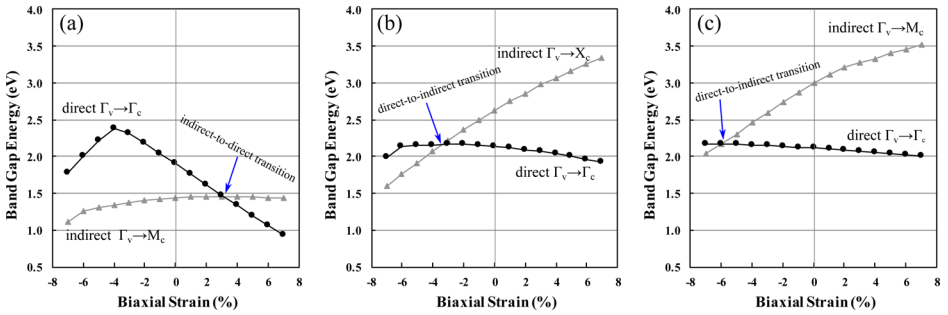

Figure 3. Direct and indirect band gap energies as a function of biaxial strain for bilayered Si NSs with (a) (111), (b) (110), and (c) (001) orientations. Γ_v represents the valence band edge at the Γ-point while Γ_c, M_c, and X_c indicate the conduction band edge at the Γ-point, *M*-point, and *X*-point, respectively.

which was validated by comparing energetics and structures for oxygen molecules reacting with Si surfaces to ab initio calculations and experimental observations.[39,40] In the simulations, a (111) Si NS with lateral dimensions of 3.92 × 3.78 nm^2 and a thickness of ∼1.0 nm (4 Si layers) was used. Before oxidation, relaxation of the Si NS was run for 100 ps at 300 K to remove any possible stress caused by a nonequilibrium surface structure. Then, up to 800 O_2 molecules were consecutively and randomly positioned one by one at a distance of 1.5 nm from the surface in intervals of 5 ps with a total simulation time of 4 ns. The oxidation temperature was set to 300 K to mimic oxidation reactions under ambient conditions. After the oxidation simulation, unreacted O_2 molecules were removed from the system. Then, an equilibration run of 30 ps at 300 K was performed to obtain the final radial distribution function. It is important to note that the present surface oxidation simulation did not consider oxygen diffusion over a long time scale due to the fundamental limit of the classical MD simulation method. However, even though the current simulation is limited to the very early stage of oxidation, it reveals that strain evolves during oxidation of very thin Si NSs.

RESULTS AND DISCUSSION

We will first present the results of bilayered Si NSs and later discuss the thickness effect. Figure 2 shows the calculated electronic band structures of unstrained bilayered Si NSs. Unstrained (111) Si NSs exhibit an indirect band gap where the conduction band minimum (CBM) is located at the *M*-point and the valence band maximum (VBM) at the Γ-point (see Figure 2a). This electronic band structure reflects that of bulk Si. However, the band gap energy of the bilayered (111) Si NS is 1.44 eV, which is about 2 times larger than that of the bulk phase, 0.61 eV. Increasing the thickness of the (111) Si NS leads to a decrease in the band gap energy. For the 10 layered (111) Si NS (about 2 nm in thickness), the band gap is calculated to 0.81 eV. The larger band gap for thinner Si NSs originates from the well-known quantum confinement effect in low-dimensional nanomaterials.[29] The band structure of the unstrained (110) Si NS reveals a direct band gap of 2.14 eV, with both the VBM and the CBM positioned at the Γ-point (Figure 2b). In the case of the (001) Si NS, we obtained a direct band gap of 2.11 eV, also at the Γ-point as shown in Figure 2c. For the (110) and (001) Si NSs, the confinement plane lies in the Γ−*M* directions. The CBM at the *M*-point is thus folded into the Γ-point,[27] leading to a direct band gap.

Imposing biaxial strain on the *xy* plane of the Si NSs significantly changes the electronic band structures and thus the band gap energies. Figure 3 shows the variation of the direct and indirect band gap energies of bilayered Si NSs with imposed biaxial strain. For the (111) Si NSs, cf. Figure 3a, the direct band gap from the valence band edge at the Γ-point to the conduction band edge also at the Γ-point exhibits a maximum of 2.38 eV at a compressive strain of −4% and shows a monotonic decrease to about 1 eV as the imposed strain goes from compressive to tensile. On the other hand, the indirect band gap from the valence band edge at the Γ-point to the conduction band edge at the *M*-point marginally increases with increasing biaxial strain from compressive (−7%) to tensile (+7%). As a consequence, a transition from indirect to direct band gap occurs at a tensile strain of +3.2%. For the (110) and (001) Si NSs, indirect band gap energies are substantially dependent on the imposed strain while the direct band gap exhibits a minor dependence. In these NSs, an indirect-to-direct band gap transition occurs at a compressive strain of −3.4% for the (110) Si NS and −6.1% for the (001) Si NS as shown in Figure 3b,c, respectively. These results show that the imposed strain induces a band gap transition regardless of the orientation of the NSs although the orientation affects a critical strain for the band gap transition. It is further noted that

DOI: 10.1021/acs.jpcc.8b02239
J. Phys. Chem. C 2018, 122, 15297−15303

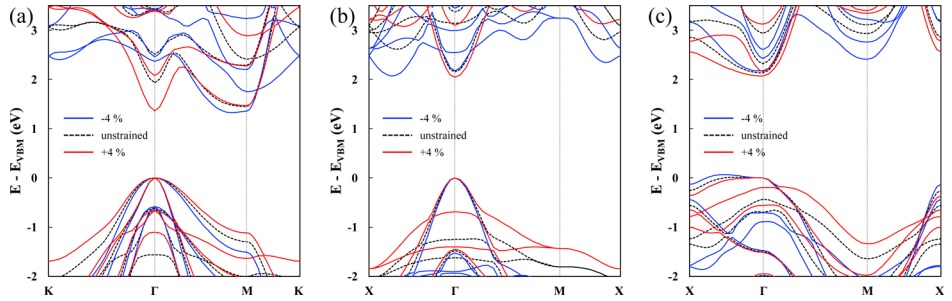

Figure 4. Band structures of geometry optimized bilayered Si NSs of (a) (111), (b) (110), and (c) (001) orientations with and without imposed biaxial strain. Dashed lines indicate the band structure of unstrained Si NSs. Blue and red lines indicate that of Si NSs with compressive and tensile strain of 4%, respectively. The band structures are shifted so that the VBM is at 0 eV in all cases.

increasing the lateral dimensions of the Si NSs enhances the direct band gap characteristics, as can be judged from the difference in energy between direct and indirect band gaps.

To understand the origin of the observed band gap transitions, we analyzed and compared the electronic band structures of the Si NSs with the imposed strain of ±4% to those of the unstrained ones. For the convenience in comparison, the band structures were shifted to align all VBMs at the Γ-point at zero energy in Figure 4. It is obvious from Figure 4a that the conduction band edge at the Γ-point of the (111) Si NS shifts downward as the strain changes from −4 to +4%. On the other hand, the conduction band edge at the *M*-point remains almost unchanged. The conduction band edge at the Γ-point becomes lower than that of the *M*-point at a critical strain of +3.2%, resulting in an indirect-to-direct band gap transition. Different behaviors were observed in the (110) and (001) Si NSs. In the case of the (110) Si NS, the conduction band edge near the *X*-point shifts upward as the imposed strain changes from −4 to +4%, while the conduction band edge at the Γ-point is insensitive to the imposed strain (see Figure 4b). Therefore, the CBM of the (110) Si NS changes from the Γ-point to a point near the *X*-point as compressive strain increases, that is, a direct-to-indirect band gap transition occurs. Similarly, the CBM of the (001) Si NS changes from the Γ- to the *M*-point with increasing compressive strain as shown in Figure 4c.

The electronic band structure changes can be understood by examining the band decomposed charge density of the conduction band edges. Figure 5a,b show the charge density plots of the conduction band edge at the Γ- and *M*-points, respectively, of the bilayered (111) Si NS as an example. The conduction band edge at the Γ-point (Figure 5a) is composed of interlayer bonding states, interlayer antibonding states and in-plane antibonding states. Figure 5b shows the conduction band edge at the *M*-point, which is also composed of bonding and antibonding states, but these states are less distinctive and more delocalized over the Si lattice. The imposed strain, which changes the atomic distances in the structure, will affect the band structure differently at different *k*-points depending on their bonding characteristics. Figure 6 shows the changes in the in-plane atomic distance, d_{IP}, and interlayer atomic distance, d_{IL} as a function of imposed strain. As the strain changes from −7 to +7%, the d_{IP} rapidly increases from 2.26 to 2.49 Å, while the d_{IL} slightly increases from 2.34 to 2.37 Å. Hence, the significant downshift of the conduction band edge at the Γ-point (see Figure 4a) can be understood by the significant increase in d_{IP}, which is in the direction of the Γ-point associated in-plane antibonding states, cf. Figure 5a. On the other hand, the

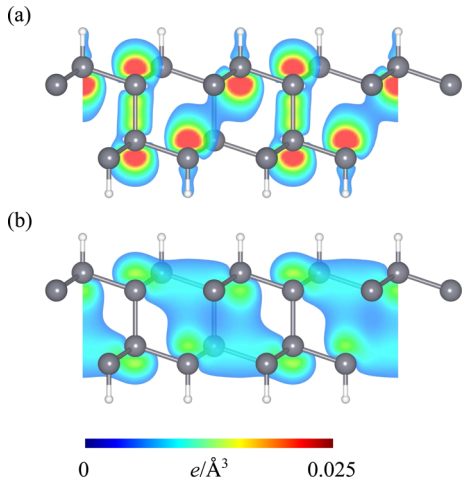

Figure 5. Band decomposed charge density of (a) the conduction band edge at the Γ-point and (b) the conduction band edge at the *M*-point.

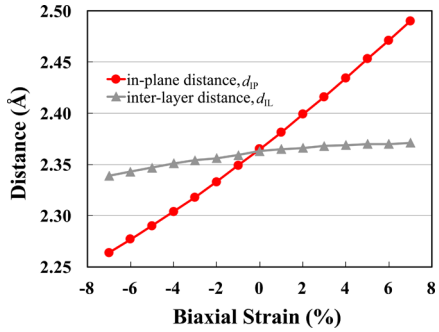

Figure 6. Changes in in-plane distance, d_{IP} and in interlayer distance, d_{IL} as a function of imposed biaxial strain for bilayered (111) Si NSs.

increase in d_{IL} is marginal and both bonding and antibonding states exist between interlayer atoms. Therefore, the effect of the interlayer distortion would be negligible on the conduction band shift at the Γ-point. At the *M*-point, the bonding states are highly delocalized and the strain induced bond distortion results only in a minor shift of the conduction band edge at this location. Similar analysis can be made to explain the indirect-to-direct band gap transitions of the (110) and (001) Si NSs. The conduction band edges at the *X*-point for (110) Si NSs and the *M*-point for (001) Si NSs are sensitive to the imposed strain (see Figure 4b,c, respectively). We found that these bands correspond to in-plane bonding states, which are stabilized at

DOI: 10.1021/acs.jpcc.8b02239
J. Phys. Chem. C 2018, 122, 15297−15303

shorter internucleus distances (see Figures S2 and S3 in the Supporting Information).

We further investigated the thickness effect on the electronic structure of the (111) Si NS. Figure 7a shows that the critical strain for an indirect-to-direct band gap transition rapidly increases from 1.1% for the monolayered Si NS to 4.2% for the four-layered Si NS. For NSs of larger thickness, the critical strain appears saturated at about 4.5%. Figure 7b shows that the energy difference of the conduction band edge between the Γ-point and the *M*-point becomes larger as the Si NSs become thicker. A larger strain is thus required to shift the conduction band edge at the Γ-point lower in energy than that of the *M*-point. The calculated thickness dependence of the electronic band structure in (111) Si NSs is consistent with previous theoretical studies on Si NWs.[27,29]

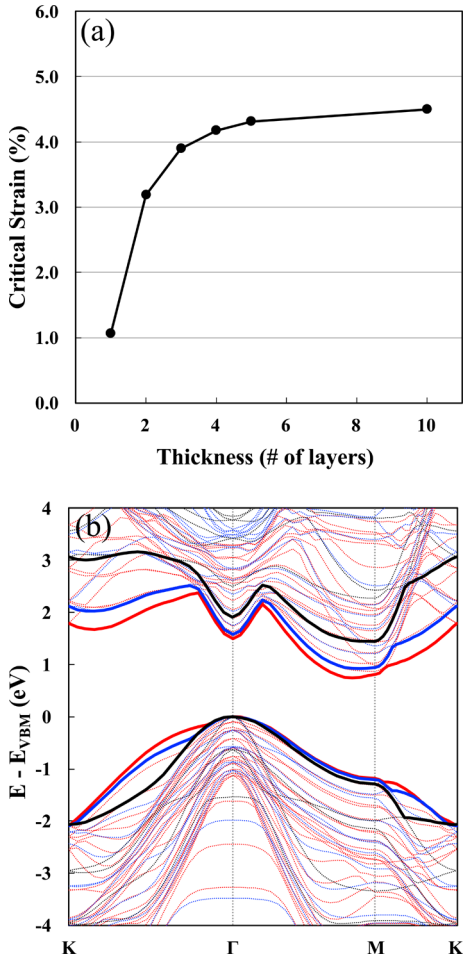

Figure 7. (a) Critical strain for indirect-to-direct band gap transition as a function of thickness for (111) Si NSs. (b) Band structures of geometry optimized Si NSs with different thickness: black, blue, and red lines indicate 2, 5, and 10 layered Si NSs, respectively. The band structures are shifted so that the VBM is at 0 eV in all cases.

Our study, using Si NSs, reveals a simple and plausible mechanism based on orbital theory and atomic structures for how the electronic band structure varies with imposed strain. Our results further provide a clue to understand the experimental observations of efficient light emission from thin (111) Si NSs.[13,14] On the basis of our calculations, an efficient light emission from unstrained (111) Si NSs cannot be expected because of its indirect band gap characteristic. However, a transition to a direct band gap may occur in the Si NS if sufficient tensile strain is imposed, either intrinsically or extrinsically. One of the most feasible ways would be surface oxidation of the Si NS. Figure 8a,b shows the atomic configuration of a four-layered Si NS before and after oxidation, respectively. The color of the atoms in Figure 8a,b represents the Mulliken charge of the atoms in the scale of the color strip at the bottom of Figure 8b. A change in color represents charge transfer between O and Si atoms as oxidation occurs. The Mulliken charge of Si and O atoms in the fully oxidized SiO_2 layer are approximately +1.4*e* and −0.8*e*, respectively, which are consistent with those of previous calculations of *α*-quartz.[39,40] At the early stage of oxidation, the dominant species formed at the interface was identified as Si−O−Si where O incorporates into Si−Si bonds because only O_2 molecules were used as an oxidant to mimic a dry oxidation process. Finally, the outer oxide layer became an amorphous structure, whereas the inner layer of Si NSs remained as unoxidized Si.

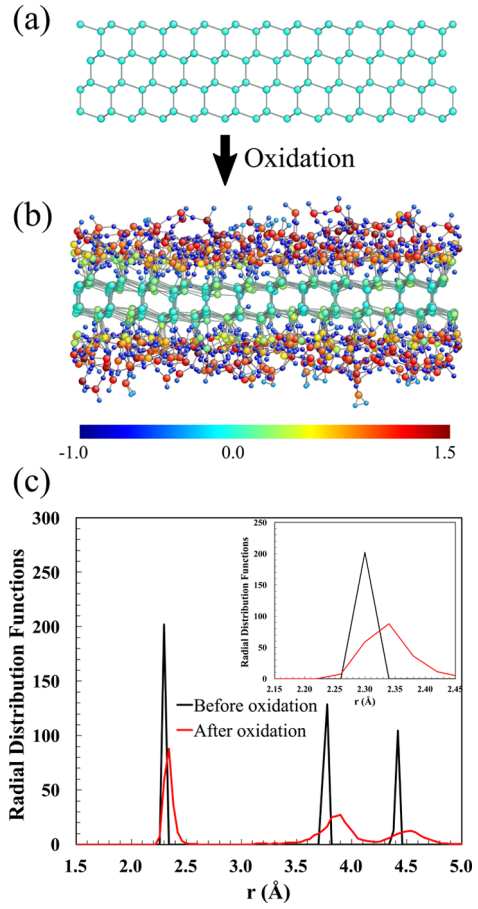

Figure 8. Atomic configuration of the four-layered Si NS (a) before and (b) after oxidation colored by the Mulliken charge distribution and (c) its corresponding radial distribution function of Si−Si bonds in the unoxidized layer.

Figure 8c shows their corresponding radial distribution function of Si−Si pairs in the unoxidized inner layer part of the Si NS. It is evident that the first nearest neighbor distance between Si in the unoxidized layer is extended from 2.30 to 2.34 Å due to surface oxidation. This increase in the interatomic distance is equivalent to a tensile strain of 1.7%. The origin of this expansion is because of the larger molar volume of SiO_2 compared to Si. A volume expansion of the unoxidized region

DOI: 10.1021/acs.jpcc.8b02239
J. Phys. Chem. C 2018, 122, 15297−15303

of Si nanomaterials has been reported previously, in both experimental[41] and theoretical[24] studies of surface oxidation. In the few nanometer scale, the inner core of the Si particle or Si NW cannot sustain the volume expansion of the surface oxide layer, and it becomes energetically more favorable for the inner Si core atoms to deform to release the stress of the surface oxide layer. Thus, our simulations of early stage surface oxidation of thin (111) Si NSs show that surface oxidation imposes tensile strain in the unoxidized inner Si layer. Even though the strain from our MD simulation is smaller than the critical values for an indirect-to-direct band gap transition in the pure Si NSs, these results qualitatively indicate that the oxidation induced tensile strain could be the cause of the indirect-to-direct band gap transition in (111) Si NSs and thus the efficient light emission. These results also suggest that the light emission can be optimized by careful tuning of the surface oxidation process. One might raise a question if the surface oxidation itself may have influences on the electronic band structures. However, because amorphous Si oxide exhibits a large band gap (>8.0 eV), one can imagine that the surface oxidation would not have a significant influence on the light emission property of Si NSs.

CONCLUSIONS

DFT calculations of strained Si NSs revealed that Si NSs yield an indirect-to-direct band gap transition as the lateral dimensions increase. This transition was observed for all considered Si NSs of different orientations. However, we found that the critical strain for an indirect-to-direct band gap transition is strongly dependent on the surface orientations and sheet thickness. For the (111) Si NS, which is the only orientation that has been synthesized experimentally so far, tensile strain is required for an indirect-to-direct band gap transition. In contrast, for (110) and (001) Si NSs, the transition occurs under compressive strain. The origin of this behavior is traced back to energy shifts in the conduction band edge at specific *k*-points being extra sensitive to the imposed strain. The most significant result of the present work is that the (111) Si NS under tensile strain has a direct band gap which could be the physical explanation of the efficient light emissions observed in previous experiments.[13,14] Furthermore, MD simulations of initial oxide growth show that surface oxidation can impose tensile strain in the unoxidised Si layers. Therefore, controlling the surface oxidation kinetics is suggested as a route to optimize and control the photonic properties of Si NSs.

ASSOCIATED CONTENT

Supporting Information

The Supporting Information is available free of charge on the ACS Publications website at DOI: 10.1021/acs.jpcc.8b02239.

Stress-strain curves for bi-layered (111), (110) and (001) Si NS and total energy changes as a function of biaxial strain in bilayered (111), (110), and (001) Si NSs; band decomposed charge density of unstrained and 4% compressed (110) and (001) Si NSs; and the in-plane and inter-layer distance changes as a function of biaxial strain in bilayered (110) and (001) Si NSs (PDF)

AUTHOR INFORMATION

Corresponding Author

*E-mail: krlee@kist.re.kr.

ORCID

Byung-Hyun Kim: 0000-0003-2493-5452

Author Contributions

⊥B.-H.K. and M.P. contributed equally.

Notes

The authors declare no competing financial interest.

ACKNOWLEDGMENTS

B.-H.K., M.P., G.K. and K.-R.L. acknowledge funding from the Nano Materials Development Program (2016M3A7B4025402). Grants from the National Research Foundation of Korea (NRF, Grant No. 2017K2A9A2A12000322) and the Swedish Foundation for International Cooperation in Research and Higher Education (STINT, Grant No. KO2016-6901) within their joint Korea-Sweden Research Cooperation program are gratefully acknowledged by B.-H.K. and K.-R.L. on the Korean side, and K.H. and P.B. on the Swedish side. This research was also funded by the Research and Development Program of Korea Institute of Energy Research (KIER) (B8-2453). The calculations were performed on resources provided by the Swedish National Infrastructure for Computing (SNIC) at UPPMAX and NSC.

REFERENCES

(1) Geim, A. K. Graphene: Status and Prospects. *Science* **2009**, *324*, 1530−1534.

(2) Fujii, S.; Ziatdinov, M.; Ohtsuka, M.; Kusakabe, K.; Kiguchi, M.; Enoki, T. Role of Edge Geometry and Chemistry in the Electronic Properties of Graphene Nanostructures. *Faraday Discuss.* **2014**, *173*, 173−199.

(3) Golberg, D.; Bando, Y.; Huang, Y.; Terao, T.; Mitome, M.; Tang, C.; Zhi, C. Boron Nitride Nanotubes and Nanosheets. *ACS Nano* **2010**, *4*, 2979−2993.

(4) Sun, W.; Meng, Y.; Fu, Q.; Wang, F.; Wang, G.; Gao, W.; Huang, X.; Lu, F. High-Yield Production of Boron Nitride Nanosheets and Its Uses as a Catalyst Support for Hydrogenation of Nitroaromatics. *ACS Appl. Mater. Interfaces* **2016**, *8*, 9881−9888.

(5) Radisavljevic, B.; Radenovic, A.; Brivio, J.; Giacometti, V.; Kis, A. Single-layer MoS_2 Transistors. *Nat. Nanotechnol.* **2011**, *6*, 147−150.

(6) Huang, Y.; Guo, J.; Kang, Y.; Ai, Y.; Li, C. M. Two Dimensional Atomically Thin MoS_2 Nanosheets and Their Sensing Applications. *Nanoscale* **2015**, *7*, 19358−19376.

(7) Nakano, H.; Mitsuoka, T.; Harada, M.; Horibuchi, K.; Nozaki, H.; Takahashi, N.; Nonaka, T.; Seno, Y.; Nakamura, H. Soft Synthesis of Single-Crystal Silicon Monolayer Sheets. *Angew. Chem., Int. Ed.* **2006**, *45*, 6303−6306.

(8) Morishita, T.; Nishio, K.; Mikami, M. Formation of Single- and Double-layer Silicon in Slit Pores. *Phys. Rev. B: Condens. Matter Mater. Phys.* **2008**, *77*, No. 081401(R).

(9) Okamoto, H.; Kumai, Y.; Sugiyama, Y.; Mitsuoka, T.; Nakanishi, K.; Ohta, T.; Nozaki, H.; Yamaguchi, S.; Shirai, S.; Nakano, H. Silicon Nanosheets and Their Self-assembled Regular Stacking Structure. *J. Am. Chem. Soc.* **2010**, *132*, 2710−2718.

(10) Sugiyama, Y.; Okamoto, H.; Mitsuoka, T.; Morikawa, T.; Nakanishi, K.; Ohta, T.; Nakano, H. Synthesis and Optical Properties of Monolayer Organosilicon Nanosheets. *J. Am. Chem. Soc.* **2010**, *132*, 5946−5947.

(11) Nakano, H.; Ikuno, T. Soft Chemical Synthesis of Silicon Nanosheets and Their Applications. *Appl. Phys. Rev.* **2016**, *3*, 040803.

(12) Ryu, J.; Hong, D.; Choi, S.; Park, S. Synthesis of Ultrathin Si Nanosheets from Natural Clays for Lithium-Ion Battery Anodes. *ACS Nano* **2016**, *10*, 2843−2851.

(13) Kim, U.; Kim, I.; Park, Y.; Lee, K.-Y.; Yim, S.-Y.; Park, J.-G.; Ahn, H.-G.; Park, S.-H.; Choi, H.-J. Synthesis of Si Nanosheets by a Chemical Vapor Deposition Process and Their Blue Emissions. *ACS Nano* **2011**, *5*, 2176−2181.

DOI: 10.1021/acs.jpcc.8b02239
J. Phys. Chem. C 2018, 122, 15297−15303

(14) Kim, S. W.; Lee, J.; Sung, J. H.; Seo, D.-j.; Kim, I.; Jo, M.-H.; Kwon, B. W.; Choi, W. K.; Choi, H.-J. Two-Dimensionally Grown Single-Crystal Silicon Nanosheets with Tunable Visible-Light Emissions. *ACS Nano* **2014**, *8*, 6556−6562.
(15) Lee, J.; Kim, S. W.; Kim, I.; Seo, D.; Choi, H.-J. Growth of Silicon Nanosheets Under Diffusion-Limited Aggregation Environments. *Nanoscale Res. Lett.* **2015**, *10*, 429.
(16) Hirschman, K. D.; Tsybeskov, L.; Duttagupta, S. P.; Fauchet, P. M. Silicon-based Visible Light-emitting Devices Integrated into Microelectronic Circuits. *Nature* **1996**, *384*, 338−341.
(17) Ng, W. L.; Lourenço, M. A.; Gwilliam, R. M.; Ledain, S.; Shao, G.; Homewood, K. P. An Efficient Room-temperature Silicon-based Light-emitting Diode. *Nature* **2001**, *410*, 192−194.
(18) Almeida, V. R.; Barrios, C. A.; Panepucci, R. R.; Lipson, M. All-optical Control of Light on a Silicon Chip. *Nature* **2004**, *431*, 1081−1084.
(19) Morishita, T.; Russo, S. P.; Snook, I. K.; Spencer, M. J. S.; Nishio, K.; Mikami, M. First-principles Study of Structural and Electronic Properties of Ultrathin Silicon Nanosheets. *Phys. Rev. B: Condens. Matter Mater. Phys.* **2010**, *82*, 045419.
(20) Wang, S.; Zhu, L.; Chen, Q.; Wang, J.; Ding, F. Stability and Electronic Structure of Hydrogen Passivated Few Atomic Layer Silicon Films: A Theoretical Exploration. *J. Appl. Phys.* **2011**, *109*, 053516.
(21) Zhang, C.; De Sarkar, A.; Zhang, R.-Q. Strain Induced Band Dispersion Engineering in Si Nanosheets. *J. Phys. Chem. C* **2011**, *115*, 23682−23687.
(22) Morales, A. M.; Lieber, C. M. A Laser Ablation Method for the Synthesis of Crystalline Semiconductor Nanowires. *Science* **1998**, *279*, 208−211.
(23) Ohta, H.; Watanabe, T.; Ohdomari, I. Strain Distribution around SiO_2/Si Interface in Si Nanowires: A Molecular Dynamics Study. *Jpn. J. Appl. Phys.* **2007**, *46*, 3277−3282.
(24) Kim, B.-H.; Pamungkas, M. A.; Park, M.; Kim, G.; Lee, K.-R.; Chung, Y.-C. Stress Evolution During the Oxidation of Silicon Nanowires in the Sub-10 nm Diameter Regime. *Appl. Phys. Lett.* **2011**, *99*, 143115.
(25) Uematsu, M.; Kageshima, H.; Shiraishi, K.; Nagase, M.; Horiguchi, S.; Takahashi, Y. Two-dimensional Simulation of Pattern-dependent Oxidation of Silicon Nanostructures on Silicon-on-insulator Substrates. *Solid-State Electron.* **2004**, *48*, 1073−1078.
(26) Lu, A. J.; Zhang, R. Q.; Lee, S. T. Stress-induced Band Gap Tuning in <112> Silicon Nanowires. *Appl. Phys. Lett.* **2007**, *91*, 263107.
(27) Hong, K.-H.; Kim, J.; Lee, S.-H.; Shin, J. K. Strain-driven Electronic Band Structure Modulation of Si Nanowires. *Nano Lett.* **2008**, *8*, 1335−1340.
(28) Shiri, D.; Kong, Y.; Buin, A.; Anantram, M. P. Strain Induced Change of Bandgap and Effective Mass in Silicon Nanowires. *Appl. Phys. Lett.* **2008**, *93*, 073114.
(29) Leu, P. W.; Svizhenko, A.; Cho, K. Ab Initio Calculations of the Mechanical and Electronic Properties of Strained Si Nanowires. *Phys. Rev. B: Condens. Matter Mater. Phys.* **2008**, *77*, 235305.
(30) Munguía, J.; Bremond, G.; Bluet, J. M.; Hartmann, J. M.; Mermoux, M. Strain Dependence of Indirect Band Gap for Strained Silicon on Insulator Wafers. *Appl. Phys. Lett.* **2008**, *93*, 102101.
(31) Baykan, M. O.; Thompson, S. E.; Nishida, T. Strain Effects on Three-dimensional, Two-dimensional, and One-dimensional Silicon Logic Devices: Predicting the Future of Strained Silicon. *J. Appl. Phys.* **2010**, *108*, 093716.
(32) Kresse, G.; Furthmüller, J. Efficient Iterative Schemes for ab initio Total-energy Calculations Using a Plane-wave Basis Set. *Phys. Rev. B: Condens. Matter Mater. Phys.* **1996**, *54*, 11169−11186.
(33) Kresse, G.; Joubert, D. From Ultrasoft Pseudopotentials to the Projector Augmented-wave Method. *Phys. Rev. B: Condens. Matter Mater. Phys.* **1999**, *59*, 1758−1775.
(34) Perdew, J. P.; Burke, K.; Ernzerhof, M. Generalized Gradient Approximation Made Simple. *Phys. Rev. Lett.* **1996**, *77*, 3865−3868.
(35) Monkhorst, H. J.; Pack, J. D. Special Points for Brillouin-zone Integrations. *Phys. Rev. B: Solid State* **1976**, *13*, 5188.
(36) van Duin, A. C. T.; Strachan, A.; Stewman, S.; Zhang, Q.; Xu, X.; Goddard, W. A., III ReaxFFSiO Reactive Force Field for Silicon and Silicon Oxide Systems. *J. Phys. Chem. A* **2003**, *107*, 3803−3811.
(37) Plimpton, S. Fast Parallel Algorithms for Short-range Molecular Dynamics. *J. Comp. Physiol.* **1995**, *117*, 1−19.
(38) Fogarty, J. C.; Aktulga, H. M.; Grama, A. Y.; van Duin, A. C. T.; Pandit, S. A. A Reactive Molecular Dynamics Simulation of the Silica-Water Interface. *J. Chem. Phys.* **2010**, *132*, 174704.
(39) Pamungkas, M. A.; Joe, M.; Kim, B.-H.; Lee, K.-R. Reactive Molecular Dynamics Simulation of Early Stage of Dry Oxidation of Si (100) surface. *J. Appl. Physiol.* **2011**, *110*, 053513.
(40) Pamungkas, M. A.; Kim, B.-H.; Lee, K.-R. Reactive Molecular Dynamic Simulations of Early Stage of Wet Oxidation of Si (001) surface. *J. Appl. Physiol.* **2013**, *114*, 073506.
(41) Hofmeister, H.; Huisken, F.; Kohn, B. Lattice Contraction in Nanosized Silicon Particles Produced by Laser Pyrolysis of Silane. *Eur. Phys. J. D* **1999**, *9*, 137−140.

DOI: 10.1021/acs.jpcc.8b02239
J. Phys. Chem. C 2018, 122, 15297−15303